INVESTIGATION ON AERODYNAMIC DESIGN OF VTOL AIRCRAFT PROPELLER

Lin-Dan Deng[1, 2], Wen-Ping Song[1,2], Jian-Hua Xu*[1,2]

[1]School of Aeronautics, Northwestern Polytechnical University, Xi'an 710072 China

[2]National Key Laboratory of Aircraft Configuration Design, Xi'an 710072 China

Abstract

VTOL (Vertical Take-off and Landing) aircraft have no runway requirement, which can greatly reduce the dependence on land resources and space resources, and take off or land anywhere. This kind of aircraft rely on the propellers to achieve vertical take-off and landing, which is the state with the largest power consumption. The propeller with higher figure of merit (FM) can save energy consumption at hovering condition, thus extending the flight time. In order to improve the FM, the in-house codes SurroOpt are carried out to obtain optimal airfoils and blades, with the in-house PMNS2D and ROTNS as flow solver. In this paper, a series of airfoils for VTOL aircraft propeller are optimized with the constraints of thickness and area to achieve geometric compatibility. The results show that the lift-to-drag ratio of the main airfoil with 10% relative thickness is improved by 3.29%. In addition, the FM of propellers are improved by 1.33%, 2.09%, and 2.77%, with 4-bladed, 5-bladed and 6-bladed, respectively.

Keywords: VTOL, propeller, airfoil, aerodynamic optimization design

1. Introduction

Vertical Take-off and Landing (VTOL) aircraft are vehicles that possess both vertical take-off and landing capabilities and efficient cruising performance. Their main advantage lies in their flexible take-off and landing, which minimizes the need for runways and significantly reduces dependence on land and space resources.

As a crucial component of the propulsion system, the aerodynamic characteristics of the lifting blade significantly impact performance at take-off and cruising conditions. The propeller with high thrust and figure of merit (FM) can support greater take-off loads and save energy during hovering. This has a major effect on key metrics of drones such as flight duration, range, and maximum payload.

The lifting blade airfoil is a fundamental component of the propeller blade, and its performance plays a crucial role in improving the efficiency and characteristics of the propeller. Jeffrey employed the inverse design method, conducting research on propeller airfoil design in conjunction with the performance of propeller-driven aircraft [1]. Xu et al. and others proposed a new series of propeller airfoil design methods that significantly enhance the aerodynamic performance of the propeller airfoil while ensuring high geometric compatibility [2].

To achieve the lifting blades with high FM, it is crucial to enhance the aerodynamic characteristics of the airfoil as well as the blade shape design. In aerodynamic blade design, the chord length, twist angle, and airfoil distribution are typically considered as key factors influencing propeller performance. The Blade Element Momentum Theory (BEMT) has been utilized in propeller aerodynamic design since early on and continues to serve as a vital tool in aerodynamic analysis. With the continuous advancement of computer technology and high-precision numerical simulations, the Reynolds Averaged Navier-Stokes (RANS) method has increasingly been applied in the aerodynamic design process or employed as a more accurate analytical tool for evaluating design proposals. Optimization design methods have become widely used in propeller blade design due to their advantages in effectively reducing design cycles, saving research costs, and

lowering the dependency on designer experience. Leusink et al. utilized a surrogate-based genetic algorithm for multi-objective optimization, improving blade twist and chord length distribution to enhance hovering and propulsion performance [3]. Li adopted helicopter rotor CLOR design concepts and methods, combining BEMT and high-precision Computational Fluid Dynamics (CFD) methods to optimize the aerodynamic layout of tiltrotor blades by determining parameters like blade profile characteristics [4]. Ng Y and others employed the NSGA-II algorithm and BEMT for multi-objective optimization design of tiltrotor blade. The optimized results show that the efficiency of propeller at cruising condition is much higher than that of the baseline blades, while the FM at hovering condition is lower than that of the baseline blades [5].

In this paper, a new airfoil series with relative thicknesses of 9%, 10%, 12%, 14%, and 16% (VP series) is designed using the in-house solver PMNS2D and optimization program SurroOpt [6][7]. The 4-bladed, 5-bladed, and 6-bladed propellers are optimized, validating the performance advantages of the new airfoil series and studying the impact of blade number on FM.

2. Flow Solver and Optimizer

2.1 Aerodynamic Analysis of Airfoil

This paper uses the in-house RANS solver--PMNS2D. Based on cell centered finite volume method, this solver is a numerical simulation program for two-dimensional flow. The spatial discretization scheme is Jameson's central scheme[8]. The time stepping method is implicit Lower-Upper Symmetric Gauss-Seidel [9]. The turbulence model is two-equation SST k-ω model [10]. γ-$\overline{Re_\theta}$ model is used for transition prediction [11].

A test case of RAE2822 at the condition of Ma=0.734, Re=6.5×10^6, α=2.86º is presented for validation of the RANS solver. Figure 1 shows the grid of airfoil for CFD simulation. Figure 2 shows that the computed pressure distribution of RAE2822 airfoil agree well with the experimental data [12].

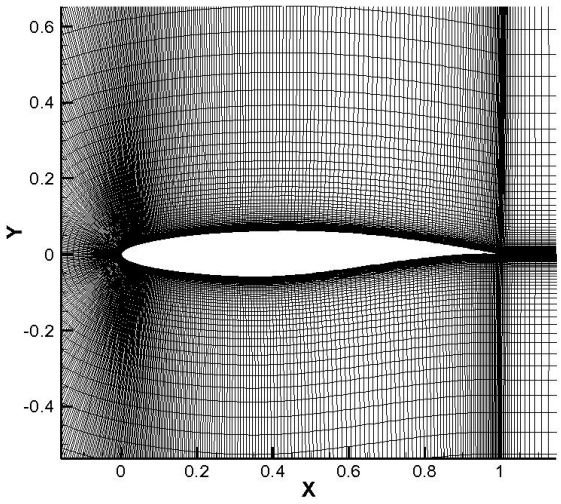

Figure 1 - The grid of airfoil for CFD simulation

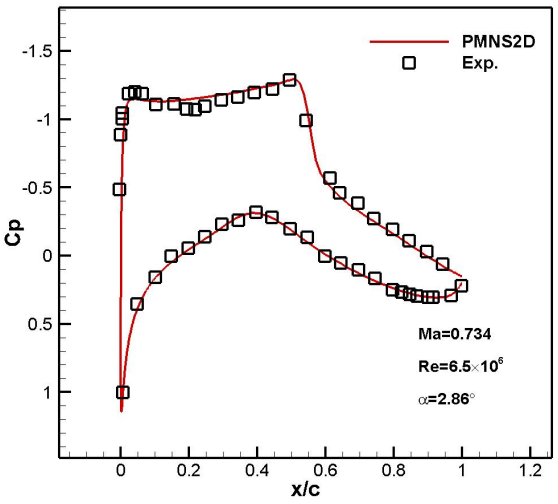

Figure 2 - The computed pressure distribution of RAE2822 airfoil agree well with the experimental data [12]

2.2 Aerodynamic Analysis of Propeller

There are two aerodynamic analysis methods used in this paper for propellers: 1) a rapid analysis program based on the classical bade-element/vortex formulation -- QPROP [13]; 2) the in-house RANS solver for flow around rotational blades -- ROTNS. For ROTNS, the spatial discretization scheme is Jameson' s central scheme [8]. The time stepping method is implicit Lower-Upper Symmetric Gauss-Seidel [9]. The turbulence model is S-A model [14].

Taking a 6-inch diameter, 2-blade propeller with an E387 airfoil section (twist angle of 15° at 75%R, as shown in Figure 3) as an example, the effectiveness of different aerodynamic analysis methods is validated. Figure 4 indicates that the calculated values from QPROP and ROTNS both agree the experimental data well, and the ROTNS calculation results are closer to the experimental values at an advance ratio of 0 (hovering condition). The reliability of both propeller analysis methods is

validated. Due to its higher computational efficiency, QPROP is used for aerodynamic analysis in the shape optimization process of lifting blades. The RASN solver --ROTNS with higher calculation accuracy is used for aerodynamic analysis of the optimized propellers.

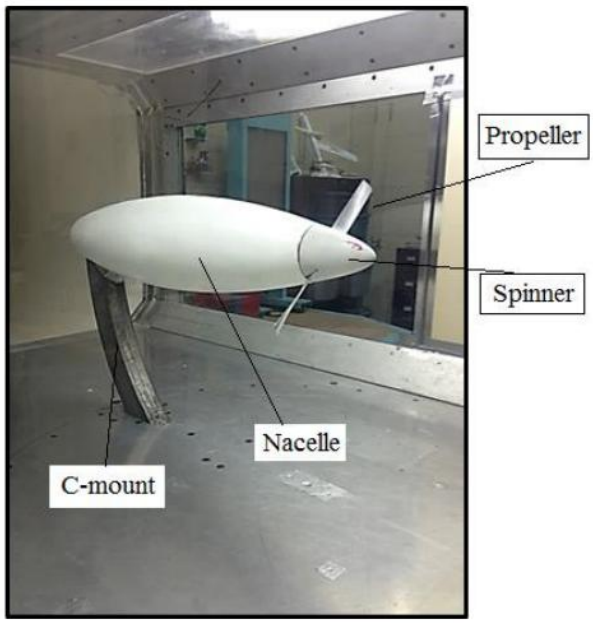

Figure 3 - A 6-inch 2-bladed propeller wind tunnel test [15]

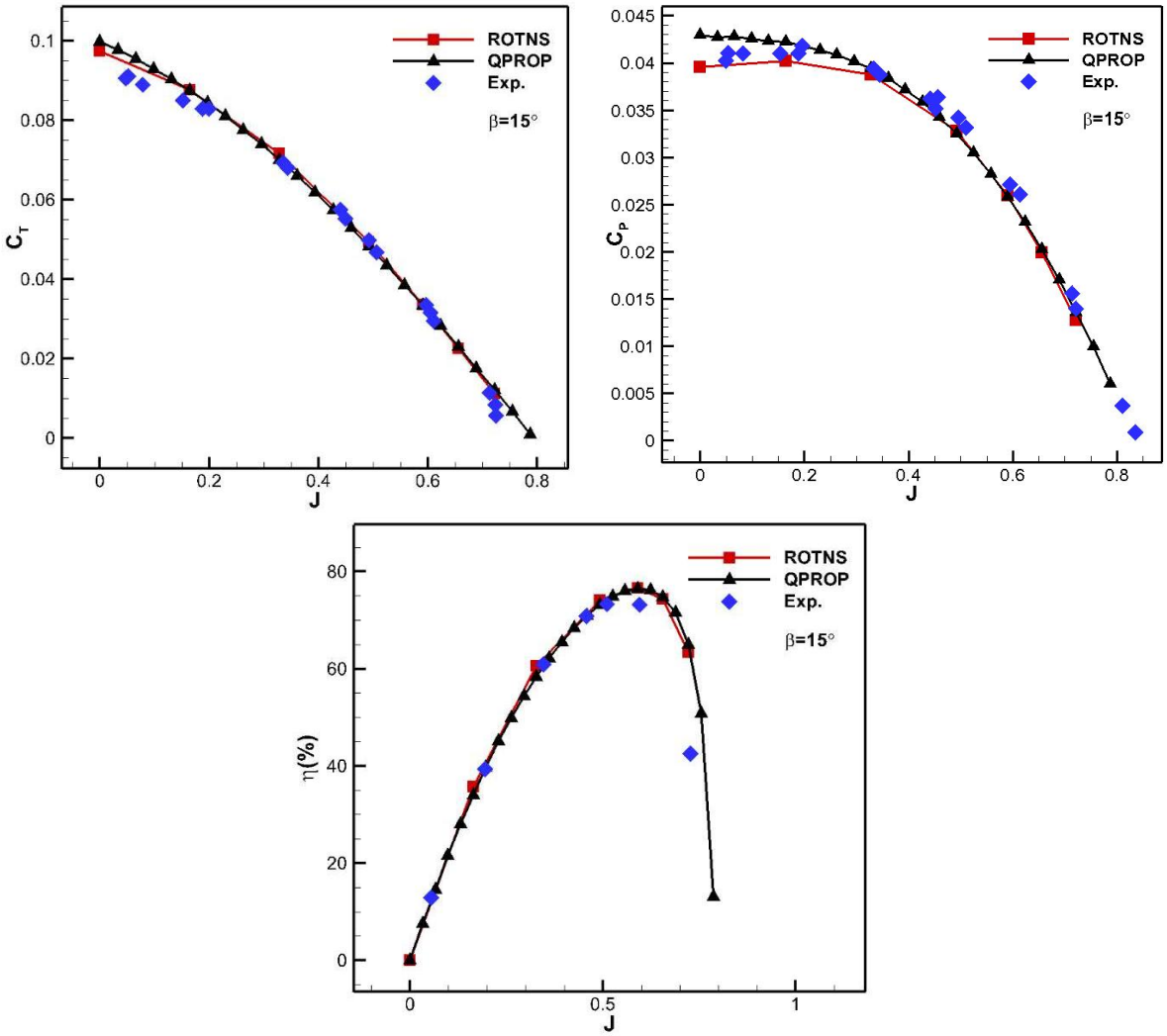

Figure 4 - The calculated values from QPROP and ROTNS both match the experimental data well ("J", "C_T", "C_P", "η" means advance ratio, thrust coefficient, power coefficient and efficiency) [15]

2.3 Optimization Method for Airfoil/Propeller

The mathematical model for airfoil aerodynamic optimization is described as follows:

$$\begin{aligned} \text{Objective} \quad & \min C_d \ (@ \text{ design } C_l) \\ \text{s.t.} \quad & thk \geqslant thk_0 \\ & area \geqslant area_0 \end{aligned} \tag{1}$$

where, "*thk*", "*area*" means the thickness and area of airfoil. "*0*" means the baseline airfoil.

The mathematical model for propeller aerodynamic optimization is described as follows:

$$\begin{aligned} \text{Objective} \quad & \min Power \\ \text{s.t.} \quad & Thrust \geq Thrust_0 \end{aligned} \tag{2}$$

where, "$Thrust_0$" means the design requirement of propeller thrust.

CST (Class function/Shape function transformation) that is presented by Kulfan from Boeing Commercial Airplanes, is used for airfoil parameterization [16].

The geometric shape of the blade is parameterized by quadratic function method. According to the characteristics of chord distribution, the distribution function is defined as a two-section quadratic function with the same peak value. The coordinate of the point with the maximum chord is (x_{cmax},$C_{R,cmax}$), the coordinate of the chord at the blade root is (x_{root},$C_{R,root}$), and the coordinate of the chord at the blade tip is (x_{tip},$C_{R,tip}$), then the chord distribution can be expressed as:

$$C_R = \begin{cases} a_1(x - x_{cmax})^2 + C_{R,cmax} \\ a_2(x - x_{cmax})^2 + C_{R,cmax} \end{cases} \tag{3}$$

where,

$$a_1 = \frac{C_{R,root} - C_{R,cmax}}{(x_{root} - x_{cmax})^2}, a_2 = \frac{C_{R,tip} - C_{R,cmax}}{(x_{tip} - x_{cmax})^2}$$

The twist distribution can be expressed in the general form of the following quadratic function:

$$\beta_R = a_\beta x^2 + b_\beta x + c_\beta \tag{4}$$

The surrogate-based in-house optimizer SurroOpt [7] is used for shape designs of airfoils and blades. The flow chart of the optimizer is shown in Figure 5.

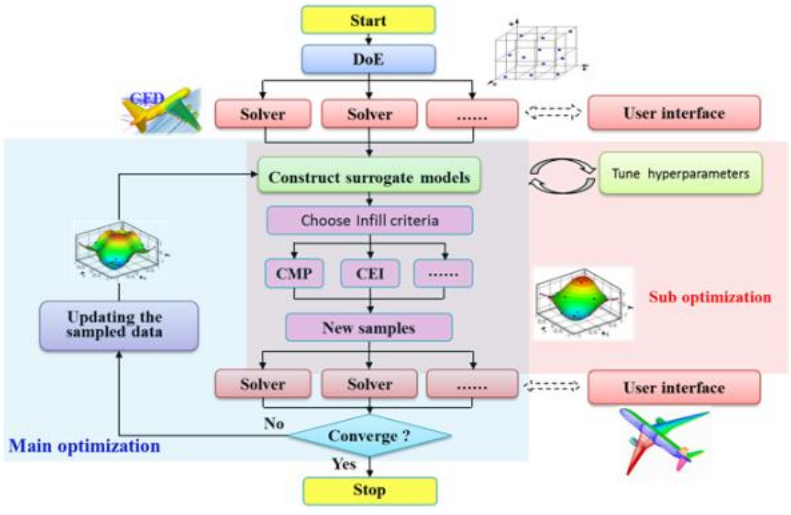

Figure 5 - The flow chart of SurroOpt [7].

3. Optimization Design of Airfoils

3.1 Design Conditions of Airfoils

The optimization at a design lift coefficient is carried out to reduce the drag in this paper, taking the PLRMS series as baseline (shown in Figure 6). Based on the requirements for VTOL aircraft lifting blades, the design conditions and requirements of airfoils of different relative thickness are

determined, as shown in Diagram 1.

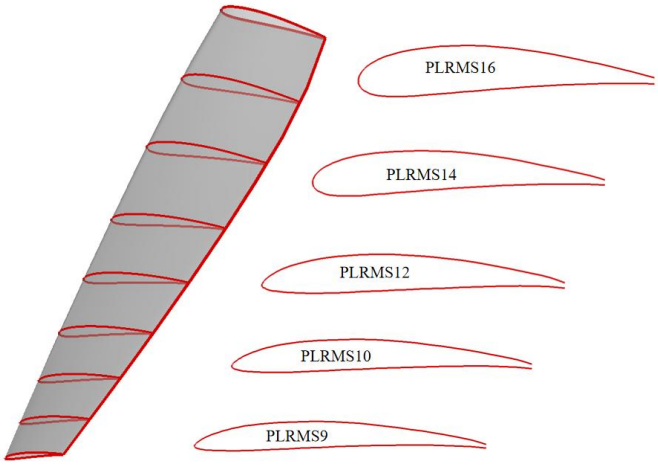

Figure 6 - The propeller blade and the PLRMS series

Diagram 1 - The design conditions and requirements of airfoils with different relative thickness

The relative thickness of airfoil (%)	Mach number	Reynolds number ($\times 10^6$)	Design lift coefficient
16	0.15	0.5	1.20
14	0.20	0.8	1.20
12	0.30	1.2	1.10
10	0.55	2.0	1.00
9	0.70	1.2	0.85

The design idea for the propeller airfoil series in this paper (shown in Figure 7) is as follows: First, an airfoil with a relative thickness of 10% is optimized based on PLRMS10 to obtain VP-10. Then, by scaling the vertical coordinates of VP-10, airfoils with relative thicknesses of 9% and 12% are optimized, resulting in VP-9 and VP-12 airfoils. Finally, airfoils with relative thicknesses of 14% and 16% are optimized by the same way.

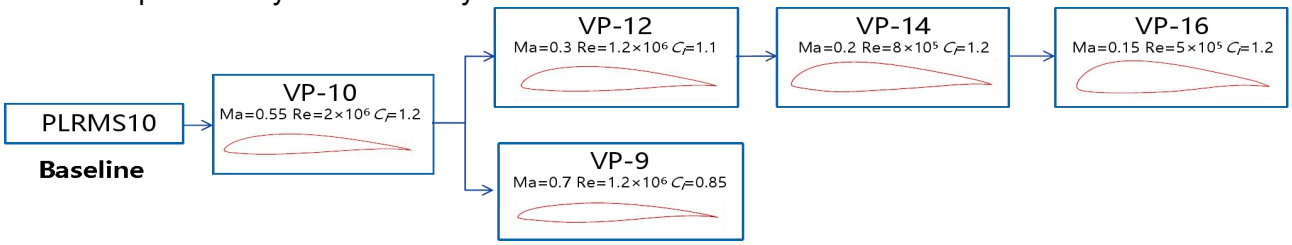

Figure 7 - The design idea of the propeller airfoil series

3.2 Design of Airfoil with 10%c Thickness

Based on PLRMS10 airfoil, the optimization design at constant lift coefficient is carried out. The design condition of the airfoil with a relative thickness of 10% is Ma=0.55, Re=2×10^6, C_l=1.0, as shown in Diagram 1.

The mathematical model for aerodynamic optimization is described as follows:

$$\begin{gathered} \text{Objective min } C_d \text{ (@ } C_l=1.0) \\ \text{s.t. } thk \geqslant 0.1 \\ area \geqslant 0.0644127 \end{gathered} \tag{5}$$

Figure 8 shows the comparison of geometric shape and pressure coefficient distribution between the baseline airfoil (PLRMS10) and the optimized airfoil VP-10. The contour of pressure distribution of baseline airfoil (PLRMS10) and optimized airfoil is demonstrated in Figure 9. The maximum thickness location of the optimized airfoil has been relocated towards the trailing edge, and the area is reduced. The aerodynamic force coefficients of baseline and optimized airfoil at the design condition are listed in Diagram 2. Compared to baseline airfoil, the drag coefficient is reduced by

3.19% and the lift-to-drag ratio increase 3.29%.

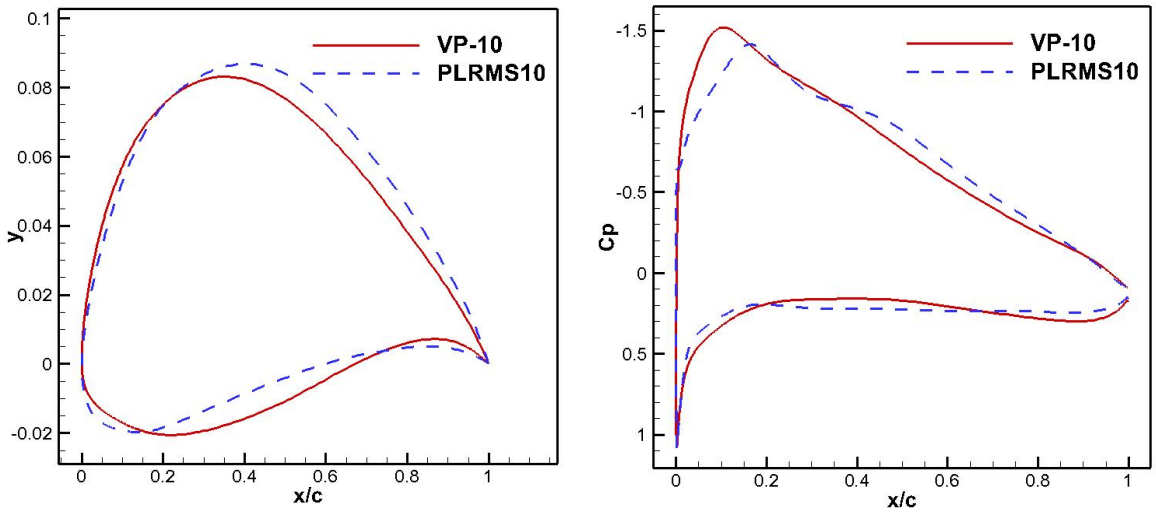

Figure 8 - Comparison of shapes and pressure distributions between baseline and optimized airfoils with 10% thickness-chord ratio

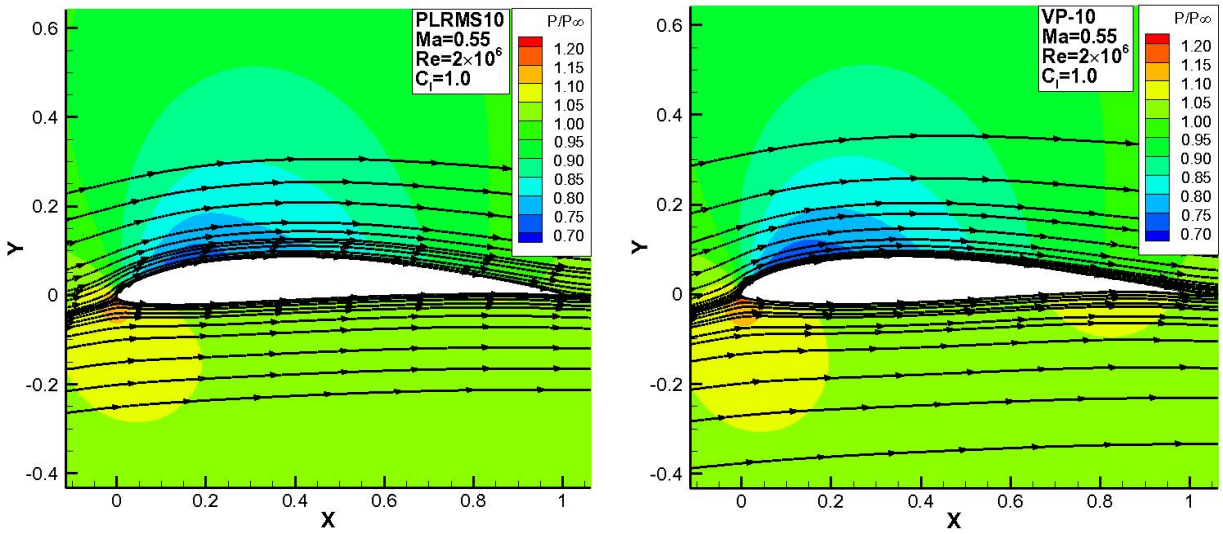

Figure 9 - The contour of pressure distribution of baseline airfoil (PLRMS10) and optimized airfoil (VP-10)

Diagram 2 - Comparison of aerodynamic force coefficients and geometric parameters between baseline and optimized airfoils(Ma=0.55, Re=2×10^6, C_l=1.0)

	C_l	C_d	C_{df}	L/D	C_m	Maximum thickness location(%c)	Area
PLRMS10	1.0	0.012144	0.007297	82.34	-0.129905	29.1	0.0644127
VP-10	1.0	0.011758	0.007217	85.05	-0.114449	31.0	0.0644130
Δ(%)	-	-3.19	-1.10	+3.29	+11.90	+6.53	-

Figure 10 shows the comparison of aerodynamic characteristics between the baseline airfoil (PLRMS10) and the optimized airfoil (VP-10). It is concluded that the slope of the lift coefficient curve increased, but the stall angle of attack and the maximum lift coefficient decreased a little; The optimized airfoil has a larger low drag coefficient range which indicates that the drag characteristic is improved; The lift-to-drag ratio of the optimized airfoil is increased significantly over the range before the maximum lift coefficient; The moment characteristics of the optimized airfoil is significantly improved.

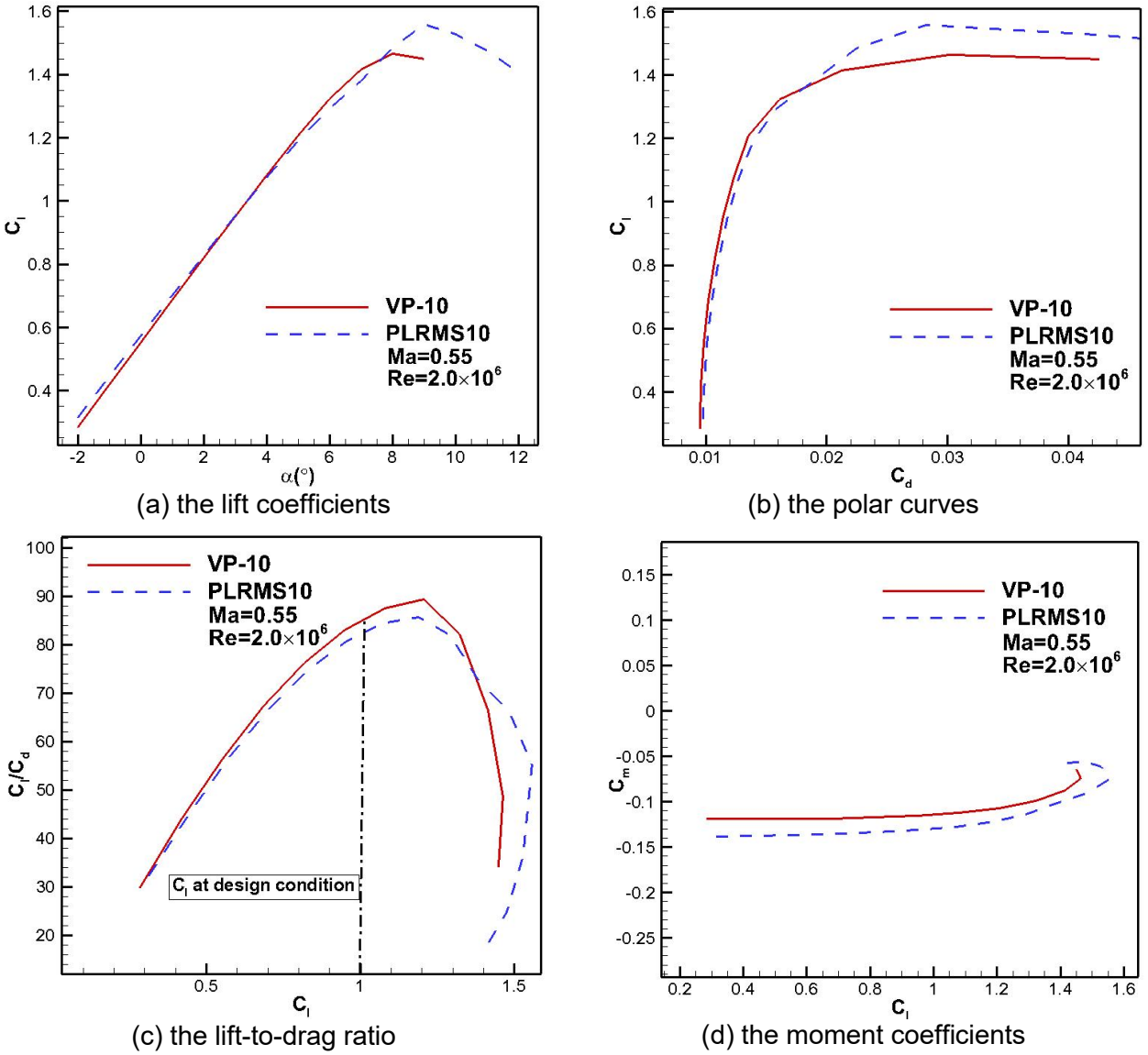

(a) the lift coefficients

(b) the polar curves

(c) the lift-to-drag ratio

(d) the moment coefficients

Figure 10 - Comparison of aerodynamic characteristics between the baseline airfoil (PLRMS10) and the optimized airfoil (VP-10)

3.3 Result of Airfoil Optimization

According to the design ideas shown in Figure 7, the optimization design of other relative thickness airfoil is completed. The new airfoil series is shown in Figure 11. The aerodynamic performance of the new airfoil series (VP) is better than that of the baseline airfoil series (PLRMS). At the design point, the lift-to-drag ratio of the new airfoil series have been improved to varying degrees. The lift-to-drag ratio of the airfoils with the relative thickness of 9%, 10%, 12%, 14% and 16% has been increased by 42%, 3%, 5%, 13% and 15%, respectively.

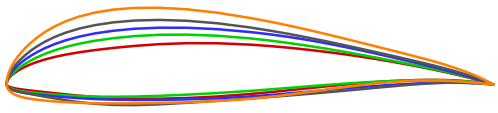

Figure 11 - The new airfoil series (VP)

4. Optimization Design of Propeller Blades

In order to obtain the propeller with higher figure of merit (FM) and illustrate the advantages of the new airfoil series (VP) in this paper, the baseline airfoil series (PLRMS) and the new airfoil series are utilized to carry out the aerodynamic design research of the blade. In the optimization design process, QPROP is used as the rapid aerodynamic analysis method of the blade. After the optimized shape is obtained, the RASN solver——ROTNS with higher calculation accuracy is used

for the propeller aerodynamic analysis.

The hovering altitude of the propeller is 0km. The velocity at hovering state is 0m/s. The radius of the propeller is 0.9m with the rotational speed range of 2500-3000 rpm.

The mathematical model for propeller aerodynamic optimization is described as follows:

$$\begin{aligned} \text{Objective} \quad & \min \textit{Power} \\ \text{s.t.} \quad & \textit{Thrust} \geq 4500\text{N} \end{aligned} \tag{5}$$

4.1 Impact of Airfoil on Propeller FM

Taking a 4-bladed propeller as an example, the blade shape optimization design is conducted by using both the PLRMS baseline airfoil series and the new VP airfoil series. The optimized blade shapes are shown in Figure 12. The chord distribution and twist distribution of the lifting blades with different airfoil sections are shown in Figure 13.

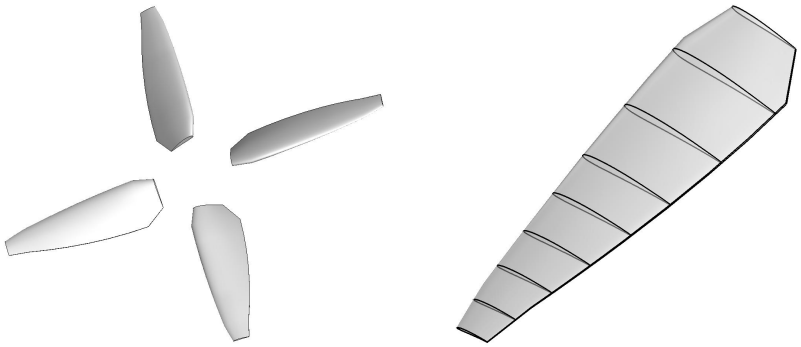

(a) the baseline airfoil series (PLRMS)

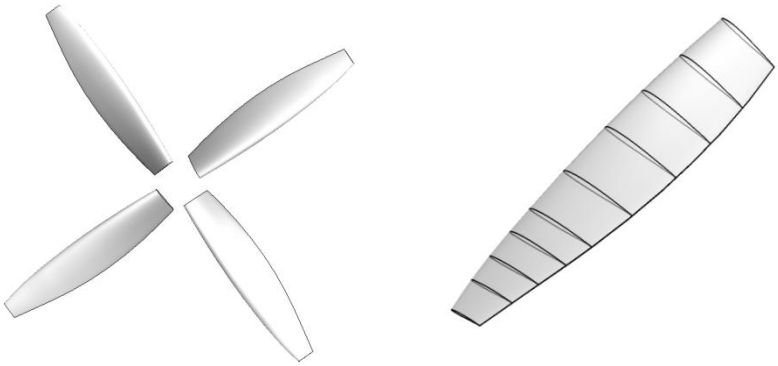

(b) the new airfoil series (VP)

Figure 12 - The geometric of optimized propellers

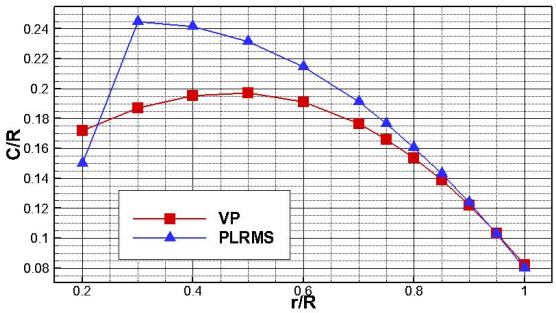

(a) chord distribution

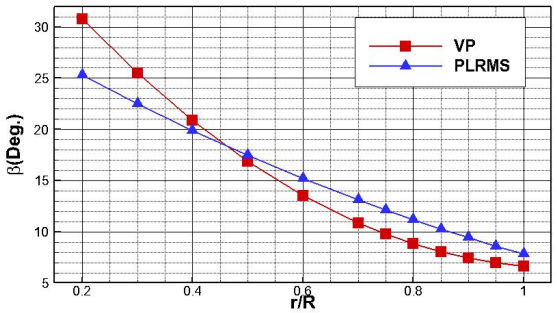

(b) twist distribution

Figure 13 - The chord and twist distributions of propellers with new airfoils (VP) and baseline airfoils (PLRMS)

Figure 14 shows the thrust-power curve of the propeller calculated by ROTNS and a detailed view around the design point. It indicates that near the design point, the power required by the new airfoil blades is less than that of the baseline airfoil blades.

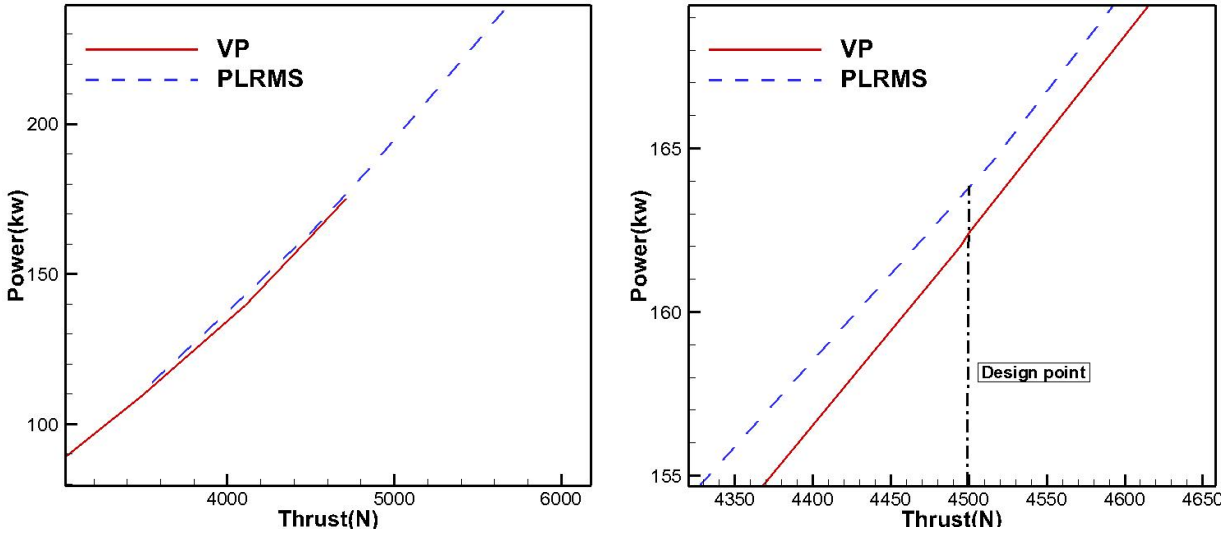

Figure 14 - The power required by the new airfoil (VP) blades is less than that of the baseline airfoil (PLRMS) blades.

Diagram 3 provides a comparison of the aerodynamic performance of the optimized blades obtained by using the two airfoil series. It shows that the FM calculated by QPROP is much higher than that calculated by ROTNS at the design point, but the trend is consistent. The QPROP results show that the FM of the new airfoil blades is improved by 3.04%, compared to the baseline airfoil blades, while the ROTNS results show an improvement of 1.33%.

Diagram 3 - Comparison of the aerodynamic performance at the design point between optimized propellers

		Rotational speed(rpm)	Thrust(N)	Torque(N·m)	Power(kW)	FM (%)
QPROP	Baseline airfoils (PLRMS)	2734	4500.0	505.8	144.8	83.50
	New airfoils (VP)	2728	4500.0	491.7	140.5	86.04
	Δ(%)	-0.22	-	-2.79	-2.97	+3.04
ROTNS	Baseline airfoils (PLRMS)	2690	4500.0	584.2	164.6	73.46
	New airfoils (VP)	2932	4500.0	528.8	162.4	74.44
	Δ(%)	+8.99	-	-9.48	-1.34	+1.33

The pressure contour and streamline of the optimized blades designed with the new VP airfoil series at the design point, as well as the pressure contour and streamline at different sections, are shown in Figure 15.

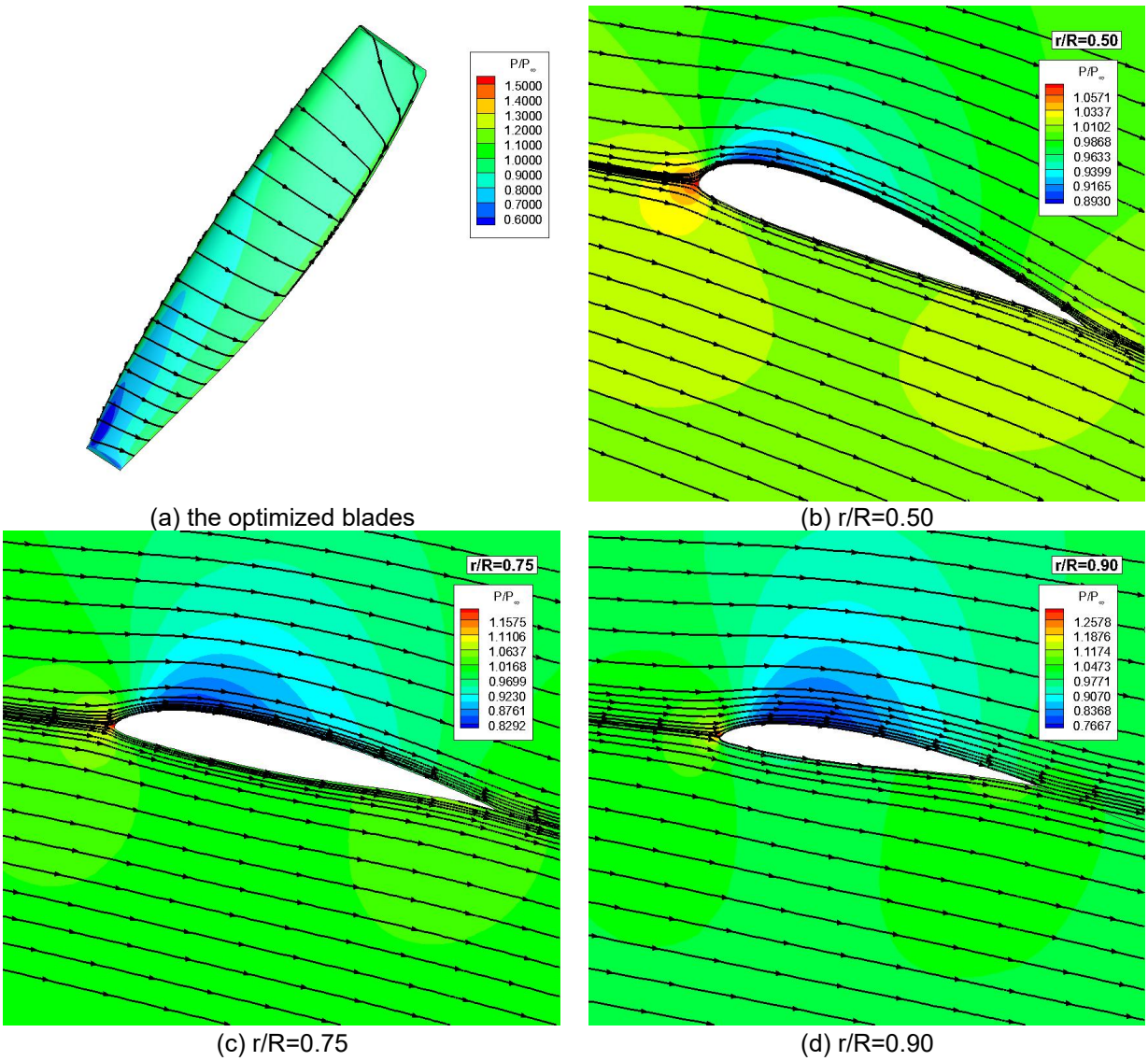

(a) the optimized blades (b) r/R=0.50

(c) r/R=0.75 (d) r/R=0.90

Figure 15 - The pressure contour and streamline of the optimized blades designed with the new VP airfoil series at different sections

4.2 Impact of Blade Number on Propeller FM

To study the impact of blade number on propeller FM, blade shape optimizations are conducted for 5-bladed and 6-bladed propellers based on the 4-bladed propeller design. By using the new VP airfoil series, the optimized blade shapes are shown in Figure 16. Figure 17 shows the thrust-power curves of the 5-bladed, 6-bladed, and 4-bladed propellers and a detailed view around the design point, calculated by ROTNS. Diagram 4 provides a comparison of the aerodynamic performance of the optimized 5-bladed propellers by using the two airfoil series, and Diagram 5 shows the aerodynamic performance comparison for the optimized 6-bladed propellers. It illustrates that the FM of the 4-bladed, 5-bladed, and 6-bladed propellers designed with the new airfoil series increased by 1.33%, 2.09%, and 2.77%, respectively, compared to those with the baseline airfoil series. Furthermore, the 5-bladed and 6-bladed propellers have higher FM.

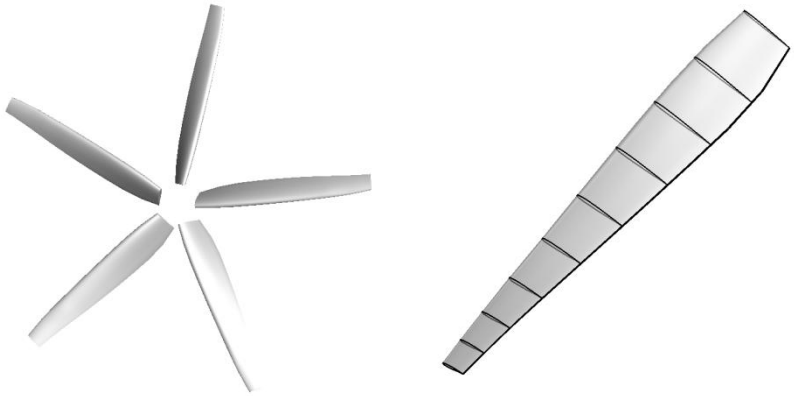

(a) 5-bladed propeller

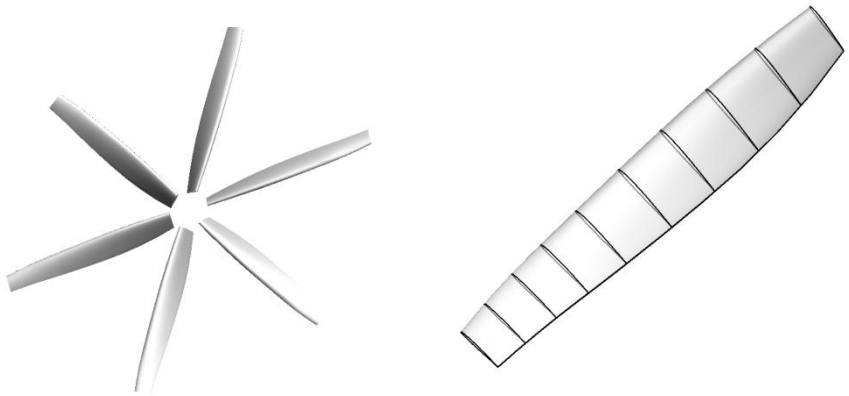

(b) 6-bladed propeller

Figure 16 - The geometric of optimized propellers

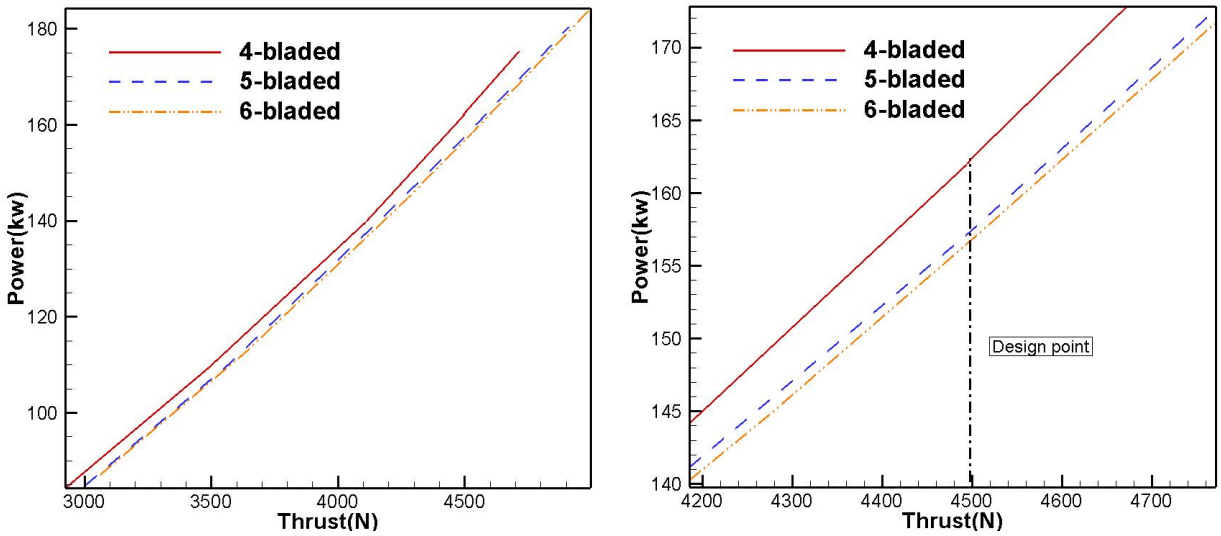

Figure 17 - The influence of blades number

Diagram 4 - Comparison of the aerodynamic performance at the design point between optimized 5-bladed propellers

		Rotational speed(rpm)	Thrust(N)	Torque(N·m)	Power(kW)	FM (%)
QPROP	Baseline airfoils (PLRMS)	2670	4500.0	512.3	143.2	84.43
	New airfoils (VP)	2705	4500.0	495.0	140.2	86.23
	Δ(%)	+1.31	-	-3.38	-2.09	+2.13

ROTNS	Baseline airfoils (PLRMS)	2600	4500.0	585.3	159.4	75.09
	New airfoils (VP)	2890	4505.0	521.0	157.7	76.66
	Δ(%)	+11.15	-	-10.98	-1.07	+2.09

Diagram 5 - Comparison of the aerodynamic performance at the design point between optimized 6-bladed propellers

		Rotational speed(rpm)	Thrust(N)	Torque(N·m)	Power(kW)	FM (%)
QPROP	Baseline airfoils (PLRMS)	2515	4500.0	543.0	143.0	84.51
	New airfoils (VP)	2708	4500.0	495.2	140.4	86.10
	Δ(%)	+7.67	-	-8.80	-1.82	+1.88
ROTNS	Baseline airfoils (PLRMS)	2490	4500.0	619.2	161.5	75.02
	New airfoils (VP)	2866	4498.0	522.0	156.7	77.10
	Δ(%)	+15.10	-	-15.69	-2.97	+2.77

5. Concluding Remarks

(1) The design requirements and approach for a series of propeller airfoils are proposed, and a new airfoil series with relative thicknesses of 9%, 10%, 12%, 14%, and 16% (named the VP series) are obtained. The aerodynamic performance of the VP series is superior to the baseline PLRMS series. The lift-to-drag ratio of the airfoils with the relative thickness of 9%, 10%, 12%, 14% and 16% has been increased by 42%, 3%, 5%, 13% and 15%, respectively.

(2) A study on the shape optimization of propellers with different blade numbers is conducted. The results indicate that the blades designed with the new airfoil series have higher FM compared to those designed with the baseline airfoil series, validating the performance advantages of the new airfoil series. Additionally, compared to the 4-bladed propeller, the 5-bladed and 6-bladed propellers exhibit higher FM.

6. Contact Author Email Address

Jian-Hua Xu *, xujh@nwpu.edu.cn.

7. Copyright Statement

References

[1] Jeffrey K, Gopalarathnam A. Incorporation of aircraft performance ponsiderations in inverse airfoil design. Journal of aircraft, Vol. 42, No. 1, pp 142-158, 2005.

[2] Xu J H, Li H J, Song W P. An aerodynamic design method of propeller airfoils with geometric compatibility as constraints. AIAA Paper: 2019-3493, 2019.

[3] Leusink D, Alfano D, Cinnella P, et al. Aerodynamic rotor blade optimization at Eurocopter--a new way of industrial rotor blade design. AIAA Paper: 2013-0779,2013.

[4] Li P. Researches on aerodynamic design and analyses on unsteady aerodynamic characteristics of the tiltrotor aircraft. Nanjing University of Aeronautics and Astronautics. 2017.

[5] Ng Y, Chen H X. Rapid aerodynamic design of prop-rotor blade with optimization. Chinese Journal of Turbomachinery, Vol. 61, No. 5, pp 19-27+4, 2019.

[6] Xu J H, Song W P and Han Z H, et al. A modified AUSM+-up scheme for simulation of flow around rotary blades. AIAA Paper: 2014-1429, 2014.

[7] Han Z H, Xu C Z, Qiao J L, et al. Recent progress of efficient global aerodynamic shape optimization using surrogate-based approach. Acta Aeronautica et Astronautica Sinica, Vol. 41, No. 05, pp 30-70, 2020 (in Chinese).

[8] Jameson A, Schmidt W, Turkel E. Numerical solution of the euler equation by finite volume methods with runge-kutta time stepping schemes. AIAA Paper: 81-1259, 1981.

[9] Han Z H. Efficient method for simulation of viscous flows past helicopter rotors and active flow control. Northwestern Polytechnical University, 2007.

[10] Menter F. Zonal two equation turbulence models for aerodynamic flows. AIAA Paper: 1993-2906, 1993.

[11] Menter F R, Langtry R B, Likki S R, et al. A correlation-based transition model using local variables—Part I: model formulation. Journal of Turbomachinery, Vol. 128, No. 3, pp 57-67, 2005.

[12] S. Nadarajah McGill University Montreal, Canada. Aerodynamic design optimization: drag minimization of the RAE2822 in transonic viscous flow.

[13] Drela M, MIT Aero & Astro. QPROP Formulation. 2006. http://web.mit.edu/drela/Public/web/qprop/qprop_theory.pdf

[14] Spalart P R, Allmaras S R. A one equation turbulence model for aerodynamic flows. AIAA Paper: 92-0439, 1992.

[15] Ghoddoussi A, Miller L S. A more comprehensive database for low Reynolds number propeller performance validations. AIAA Paper: 2016-3422, 2016.

[16] Kulfan B M. Universal parametric geometry representation method. Journal of Aircraft, Vol. 45, No. 1, pp. 142-158, 2008.